Pramana – J. Phys. (2019) 93:73
https://doi.org/10.1007/s12043-019-1831-2

Modelling and characterisation of the noise characteristics of the vertical cavity surface-emitting lasers subject to slow light feedback

HAMEEDA R IBRAHIM[1,*], MOHAMED S ALGHAMDI[2], AHMED BAKRY[2], MOUSTAFA AHMED[2,3] and FUMIO KOYAMA[1]

[1]Laboratory for Future Interdisciplinary Research on Science and Technology, Tokyo Institute of Technology, Yokohama 226-8503, Japan
[2]Department of Physics, Faculty of Science, King Abdulaziz University, 80203, Jeddah 21589, Saudi Arabia
[3]Department of Physics, Faculty of Science, Minia University, Minia 61519, Egypt
*Corresponding author. E-mail: hameedaragab@gmail.com

MS received 16 February 2019; revised 27 April 2019; accepted 31 May 2019

Abstract. This paper introduces the modelling and characterisation of the noise properties of the vertical cavity surface-emitting laser (VCSEL) coupled in lateral direction with a passive cavity. This design of VCSEL with this transverse coupled cavity (TCC) is proposed for high-speed photonics. We introduce comprehensive simulations on the influence of the induced lateral slow light feedback on the relative intensity noise (RIN) and carrier-to-noise ratio (CNR). The proposed model incorporates multiple round trips of slow light in the TCC as time delay light in the rate equations of the VCSEL. The obtained results are compared with those of the conventional VCSEL. We show that the noise performance of the TCC-VCSEL is optimised when the VCSEL exhibits stable continuous wave (CW) operation under strong slow light feedback and the TCC length is smaller than 8 μm and between 11 and 13 μm. When strong slow light induces unstable regular and/or irregular oscillations, RIN is enhanced and CNR is lowered.

Keywords. Carrier-to-noise ratio; noise; slow light; feedback.

PACS Nos 74.40.De; 05.40.Ca; 42.55.−f

1. Introduction

The advantages of small size, low cost, high speed, low power consumption and the possibility of fabrication into arrays [1,2] have made vertical cavity surface emitting lasers (VCSELs) key radiation sources in modern applications, such as the radios over fibre (RoF) networks. Noise is a primary factor affecting the performance of VCSELs and their applications. In semiconductor lasers, noise is essentially generated due to the spontaneous emission, which is the seed of the stimulated emission [3]. This noise could be amplified when the laser operates under optical feedback (OFB) due to an external reflector. This OFB noise is dependent on the coupling and phase of the re-injected radiation into the active region [4,5]. Variation in these OFB parameters can display a variety of dynamic behaviours of the laser along a variety of routes to chaos [4–6]. On the other hand, OFB was used effectively to improve the characteristics of VCSELs, e.g., to increase the modulation bandwidth [7,8], to narrow the emission linewidth [9,10], to stabilise the lasing mode [11], and to reduce the modulation-induced chirp [12]. These are the reasons for which VCSEL under OFB is a rich subject for research; see e.g. ref. [12] and its citations.

Recently, Dalir and Koyama [13,14] demonstrated a novel scheme of VCSEL integrated with an ultra-compact transverse coupled cavity (TCC) for boosting the bandwidth of VCSEL up to 60% to that of the conventional VCSEL. Also, they confirmed experiment bandwidth beyond 29 GHz [15,16]. The measured light vs. current characteristics and lasing spectra of this novel TCC-VCSEL demonstrated coherent coupling of the active and coupled cavities. Theoretical studies predicted that the slow light transverse feedback induces enhancement of the modulation bandwidth up to 70 GHz [17]. Investigation of noise properties of the TCC-VCSEL due to the induced slow light feedback is essential to evaluate the noise performance of the device.

Published online: 08 August 2019

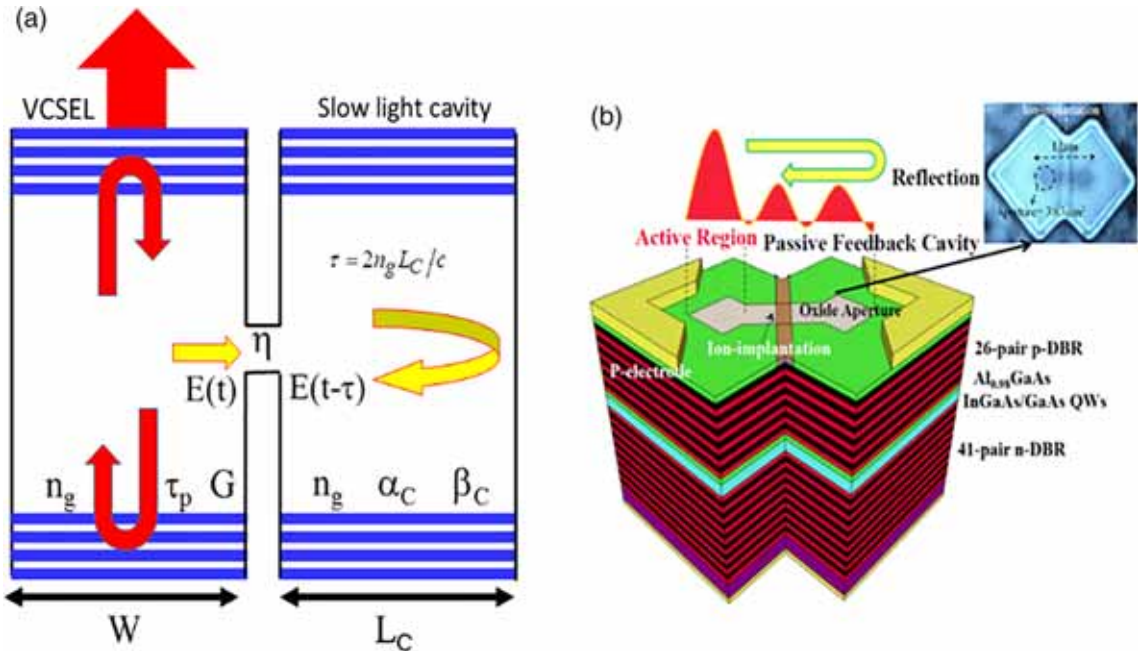

Figure 1. Schematic of (**a**) the theoretical model and (**b**) transverse-coupled cavity VCSEL.

Lang and Kobayashi [18] incorporated the OFB effect in the standard rate equations of semiconductor lasers by adding a time-delayed term [11,12]. Although this model is applicable up to moderate strengths of OFB, it was commonly followed by theoretical groups. Abdulrhmann *et al* [19] improved the time-delay model of Lang and Kobgyashi [18] by counting the round trips of laser light in the feedback cavity applied this model to classify laser operation and dynamics under strong OFB. This model was adopted to study the TCC-VCSEL noise associated with analogue modulation [20].

This paper is dedicated to investigate intensity noise due to slow light feedback in TCC-VCSELs and optimise the design parameters and operating conditions. The slow light feedback is modelled by a time-delay rate equation model suitable for strong feedback. The model also includes the optical loss and phase delay in every round trip along the TCC. VCSEL dynamics are classified based on the bifurcation diagram, and the noise is assessed by both carrier-to-noise ratio (CNR) and the Fourier spectrum of relative intensity noise (RIN). The noise is evaluated also in terms of the low-frequency level of RIN, LF-RIN (the average value of RIN when the frequency is lower than 200 MHz). We investigate the dependency of these noise properties on the coupling ratio of the slow light and length of the TCC.

2. Theoretical model

The design of the proposed TCC-VCSEL is sketched in figure 1a and the schematic cross-sectional view of the TCC-VCSEL is plotted in figure 1b. The VCSEL is integrated in the lateral direction with a TCC of length L_C through a bow-tie oxide aperture [13]. Light is confined vertically in the VCSEL cavity, and so light is guided in a zig-zag path and ambulates perpendicularly in the TCC in the form of slow light. That is, light travels perpendicular in the lateral coupled waveguide with a slower group velocity of $v_g = c/n_g$, where c is the speed of light in vacuum and $n_g = fn$ is the group index with n being the average refractive index and f being the slow factor of light [13]. The delay time of slow light feedback due to one round trip in the TCC is $\tau = 2n_gL_C/c$. During every round trip in the TCC, the slow light suffers the loss of $\exp(-2\alpha_C L_C)$ and a phase delay of $\exp(-2j\beta_C L_C)$. $\alpha_C = f\alpha_m$ and $\beta_C = 2\pi n/(\lambda f)$ are the optical loss and propagation constant, where α_m is the material loss. Then the slow light is partially injected into the primary cavity with a coupling ratio η. We treat the slow light feedback as the time delay of slow light due to the multiple round trips in the TCC. The modified time-delay rate equations are then given by

$$\frac{dN}{dt} = \frac{\eta_i}{e} I(t) - \frac{N}{\tau_s} - \Gamma G S + f_N(t), \quad (1)$$

$$\frac{dS}{dt} = \left[\Gamma G - \frac{1}{\tau_p} + \frac{v_g}{W}\ln|U|\right] S + \Gamma R_{sp} + f_S(t), \quad (2)$$

$$\frac{d\theta}{dt} = \frac{1}{2}\left(\alpha\Gamma\frac{a}{V}(N - N_{th}) - \frac{c}{n_g W}\varphi\right) + f_\theta(t). \quad (3)$$

These equations stand for the electron number $N(t)$, photon number $S(t)$ and optical phase $\theta(t)$, respectively.

G is the optical gain. Other parameters are: a is the tangential gain, V is the volume of the active layer, N_T is the electron numbers at transparency, ε is the gain suppression coefficient, Γ is the confinement factor, τ_p is the photon lifetime, η_i is the injection efficiency, τ_s is the carrier lifetime, R_{sp} is the spontaneous emission factor and N_{th} is the electron number at the threshold. The function $U = |U|e^{j\varphi}$ is a complex time-delay feedback function and is given by

$$U = 1 + \frac{\eta}{1-\eta}\sum_{p}\sqrt{1-\eta}^{p}\, e^{-2p\alpha_C L_C} e^{-j2p\beta_C L_C} \times\sqrt{\frac{S(t-p\tau)}{S(t)}} e^{j\theta(t-p\tau)-j\theta(t)}, \quad (4)$$

where $\theta(t) - \theta(t - p\tau)$ represents the deviation in the optical phase due to chirping in round p.

The last terms $f_N(t)$, $f_S(t)$ and $f_\theta(t)$ in eqs (1)–(3) represent the Langevin noise sources that describe the intrinsic fluctuations in $N(t)$, $S(t)$ and $\theta(t)$, respectively, and are given by [3]

$$f_S(t) = \sqrt{\frac{2R_{sp}\Gamma S(t)}{\Delta t}}\cdot x_s, \quad (5)$$

$$f_N(t) = \sqrt{\frac{2N(t)}{\tau_s \Delta t}}\cdot x_n - \sqrt{\frac{2R_{sp}S(t)}{\Delta t}}\cdot x_s, \quad (6)$$

$$f_\theta = \sqrt{\frac{R_{sp}\Gamma}{2S(t)\Delta t}}\cdot x_\theta. \quad (7)$$

RIN is then calculated as the frequency Fourier transform of the time fluctuations $\delta S(t)$ of the photon number $S(t)$ as [21]

$$\mathrm{RIN} = \frac{1}{S_{av}^2}\left\{\frac{1}{T}\left|\int_0^T \delta S(t)\, e^{-j2\pi f\tau} d\tau\right|^2\right\}, \quad (8)$$

where T is the sampling period and S_{av} is the corresponding time average of $S(t)$.

3. Numerical methodology

The fourth-order Runge–Kutta algorithm is applied to integrate rate equations (1)–(3) using a time step as short as $\Delta t = 0.2$ ps. The integration is first done for the solitary VCSEL ($\eta = 0$) between $t = 0$ and τ, and the obtained values of $S(t)$ and $\theta(t)$ are then used for further integration of the time-delayed version of the rate equations. We considered six round trips ($p = 1, 2, \ldots, 6$) in the integration. The simulated results on noise have minor changes when counting more round trips. The data sampled for the characterisation of laser dynamics and noise are collected after the laser operation is stabilised [22]. We apply the numerical values of the VCSEL parameters given in table 1 [23]. Generation of the noise sources $f_N(t)$, $f_S(t)$ and $f_\theta(t)$ at each integration step is described in [4] using a set of uniformly distributed random numbers in the Box–Muller approximation [24]. The frequency content of RIN is then calculated by applying fast Fourier transform (FFT) to eq. (8) as in [25]

$$\mathrm{RIN} = \frac{1}{S_{av}^2}\frac{\Delta t}{T}\left|\mathrm{FFT}\left[\delta S(t_i)\right]\right|^2. \quad (9)$$

The noise content of the signal is also characterised in terms of CNR, which is calculated from the statistics of the time variation of $S(t)$ as

$$\mathrm{CNR} = \frac{S_{av}^2}{\left\langle \delta S(t_i)^2\right\rangle}. \quad (10)$$

Table 1. Definition and numerical values of the VCSEL parameters [23].

Parameter	Value
Refractive index of the active region (n)	3.3
Material loss of the active region (α_m)	1000 m^{-1}
Slow factor (f)	50
Volume (V)	1.76×10^{-19} m^3
Width of the VCSEL cavity (W)	4 μm
Differential gain (a)	3.64×10^{-12} m^3 s^{-1}
Confinement factor (Γ)	0.0382
Electron number at transparency (N_T)	3.17×10^5
Gain suppression coefficient (ε)	1.5×10^{-5} s^{-1}
Photon lifetime (τ_{ph})	2 ps
Spontaneous emission (R'_{sp})	1.16×10^{10} s^{-1}
Injection current (I)	2 mA
Injection efficiency (η_i)	0.8
Electron lifetime (τ_s)	1.5 ns
Linewidth enhancement factor (α)	2
Injection current	2 mA

4. Results and discussion

4.1 *Characteristics of TCC-VCSELs' dynamic states*

We use bifurcation to examine various dynamic states of the TCC-VCSEL as a function of the slow light feedback strength. The diagram is simulated by collecting the peaked photon number S_{peak} normalised by the corresponding averaged photon number S_{av} at each value of the coupling ratio η. In this case, we dropped the noise

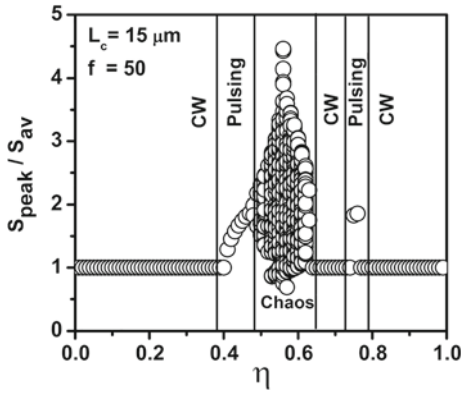

Figure 2. Bifurcation diagram of $S_{\text{peak}}/S_{\text{av}}$ as a function of the coupling ratio η when $L_{\text{C}} = 15\,\mu$m.

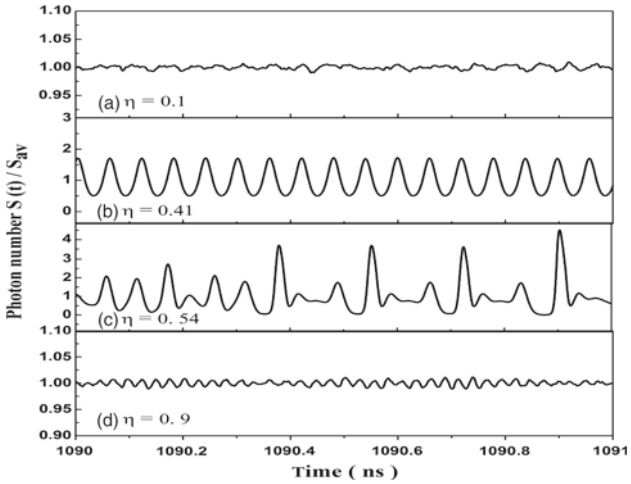

Figure 3. Typical characteristics of (**a**) CW ($\eta = 0.1$), (**b**) pulsing ($\eta = 0.41$), (**c**) chaos ($\eta = 0.54$) and (**d**) CW ($\eta = 0.9$). $L_{\text{C}} = 15\,\mu$m.

sources from rate equations (1)–(3) to gain insight into the deterministic influence of slow light on the laser dynamics. Figure 2 plots the obtained bifurcation diagram when the length of the TCC is $L_{\text{C}} = 15\,\mu$m. The figure indicates that the laser operates in stable CW operation in the regime of weak OFB with $\eta < 0.35$. This CW operation is represented in the figure as single points at $S_{\text{peak}}/S_{\text{av}} = 1$. By a further increase of OFB, the TCC-VCSEL enters a regime of unstable operation following a route to chaos. This route begins with period-1 oscillation when $\eta = 0.38$, which is represented by single points with $S_{\text{peak}}/S_{\text{av}} > 1$. These points then bifurcate into a torus (multiple bifurcation points) attracting the laser into chaotic dynamics when η is larger than 0.48. By increasing η beyond the chaos regime, the TCC-VCSEL again attains the CW operation, except over a narrow range of $0.72 < \eta < 0.78$ in which the TCC-VCSEL exhibits unstable pulsing operation. In this case, the laser is coupled to one of the resonance modes of the TCC.

Figures 3 and 4 plot the time trajectories of $S(t)$ and the frequency spectrum of RIN, respectively, that characterise the investigated states of the dynamics which includes CW operation, chaos and pulsation. These figures correspond to $\eta = 0.1$ (weak OFB), $\eta = 0.41$ and 0.54 (intermediate OFB) and $\eta = 0.9$ (strong OFB). Figures 3a and 4a correspond to the CW operation. Figure 3a shows the time fluctuations of $S(t)$ around S_{av}. Figure 4a indicates that the RIN spectrum is nearly similar to that of the VCSEL without feedback (dashed spectrum); it exhibits an enhanced peak around the relaxation oscillation frequency f_{r}. This means that the slow light feedback is not robust enough to alter the relaxation oscillation frequency of the laser. The spectrum has a white noise in the low frequency regime with an average noise level of LF-RIN $= -168$ dB/Hz.

Figures 3b and 4b characterise the periodic oscillations induced by the intermediate level of slow light feedback with $\eta = 0.41$. Figure 3b shows period-1 oscillations with a duration of $\sim 1/f_{\text{r}}$, where the slow light feedback releases the damping effect on the relaxation oscillations of the VCSEL. Figure 4b indicates that the RIN spectrum exhibits sharp peaks around a frequency comparable to f_{r} and another lower peak at the second harmonic frequency. In this case, LF-RIN is 15 dB/Hz above that of the VCSEL.

Figures 3c and 4c characterise the most noisy operation, or chaos dynamics, induced due to mode competition in both VCSEL and feedback cavities [26] when $\eta = 0.54$. Figure 3c shows that the TCC-VCSEL displays irregular time variation of $S(t)$. Figure 4c plots the RIN spectrum of the noisy operation under a moderate range of OFB, $\eta = 0.54$, showing that the whole noise spectrum is 40 dB/Hz higher than the RIN spectrum of the CW state. The relaxation oscillation peak is suppressed and there are no clear relationships among frequencies of the small peaks of the spectrum. These characteristics are typical features of chaotic dynamics [18,19].

Figures 3d and 4d are concerned with the stable CW operation attained by the TCC-VCSEL in the regime of strong OFB of $\eta = 0.9$. Similar to the CW operation under weak feedback shown in figure 3a, figure 3d shows fluctuations of $S(t)$ around its average value S_{av}. However, the fluctuations become faster in this case, indicating that the dynamics of the TCC-VCSEL are controlled by one of the oscillating modes of the TCC. These results are manifested in the RIN spectrum of figure 4d, which has a level of LF-RIN close to that of the conventional VCSEL. The RIN spectrum also

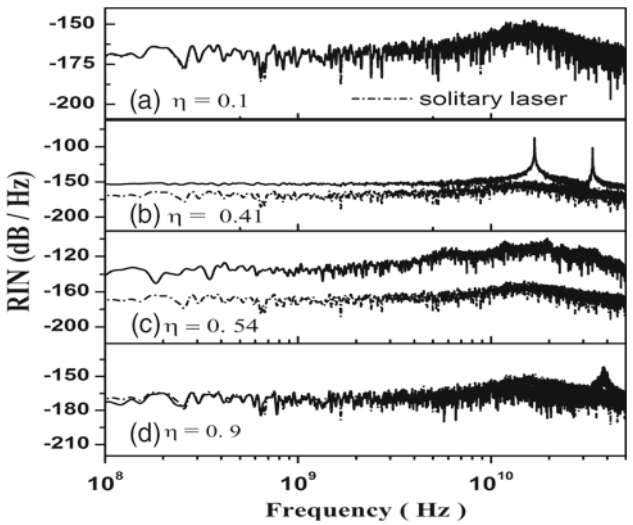

Figure 4. RIN spectrum of (**a**) CW ($\eta = 0.1$), (**b**) pulsing ($\eta = 0.41$), (**c**) chaos ($\eta = 0.54$) and (**d**) CW ($\eta = 0.9$). RIN spectrum of solitary laser is plotted by a dashed line for comparison. $L_C = 15\,\mu$m.

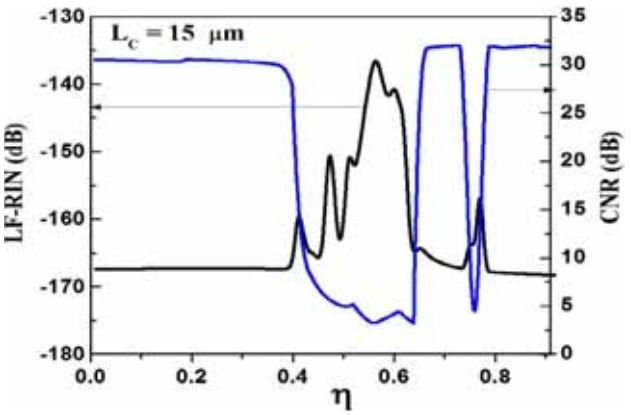

Figure 5. Variation of LF-RN with η when $L_C = 15\,\mu$m. The corresponding variation of CNR is plotted on the right-hand axis.

exhibits a peak around $f = 39$ GHz, which belongs to a resonance mode in the TCC.

4.2 *Low-frequency noise and CNR*

We characterise the noise properties according to the dynamic types shown in figure 2. Figure 5 plots the variations of LF-RIN (on the left axis) and CNR (on the right axis) with the variations of the coupling ratio η. The figure shows that both LF-RIN and CNR are nearly constant at -168 dB/Hz and 33 dB, respectively, under stable CW operation in the regime of weak feedback. When the TCC-VCSEL becomes unstable under the period-1 oscillations ($0.38 < \eta \leq 0.48$), LF-RIN increases and CNR decreases. This behaviour of LF-RIN and CNR enhances with further increase of η because of the attraction to the chaos state. The maximum value of LF-RIN is -135 dB/Hz, while the minimum value of CNR is 4 dB. The noise level increases with the increase of η, and the increase is remarkable when the operation is chaotic. When $\eta > 0.63$, LF-RIN drops to values even lower than that of the CW operation under weak feedback, while CNR recovers to higher levels of 34 dB. That is, the CW operation of the TCC-VCSEL becomes more stable. Within the regime of unstable pulsing oscillation ($0.72 < \eta < 0.78$), LF-RIN increases, reaching -158 dB/Hz while CNR drops and becomes 5 dB. These results indicate that the signal quality of the TCC-VCSEL is improved the most and the noise is reduced the most in the regime of strong slow light feedback, which could be due to the increase in light intensity in the VCSEL cavity and/or improvement of operation stability.

It is technically important to examine the validity of counting six round trips of slow light within the feedback cavity in the present noise calculations. In figure 6, we re-plot the results on LF-RIN and CNR of figure 5 when counting one, six and nine round trips. As shown in the figure, large differences are seen in the LF-RIN and CNR data when considering only one round trip, whereas considering six and nine round trips result in closed LF-RIN data and same CNR data. These results confirm the termination of the summation on the round trips in eq. (4) up to the sixth round to reduce the calculation time.

It is well known that the length of the feedback cavity has a remarkable influence on the dynamics of semiconductor lasers [19]. It is then necessary to illustrate how the TCC length L_C affects the noise properties of the TCC-VCSEL. Figures 7a and 7b, respectively plot the dependence of both RIN and CNR on L_C, under different feedback strengths of $\eta = 0.1$, 0.4 and 0.9. L_C varies between 3 μm (shorter than the primary cavity width W) and 15 μm (more than three times higher than W). The figure shows that regardless of the value of η, when the TCC cavity is shorter than $L_C = 8\,\mu$m, the values of both CNR and LF-RIN are comparable to those of the conventional VCSEL and no perceptible excess noise is seen. In this case, the TCC-VCSEL operates in stable CW under different coupling strengths. The same situation applies to the length range of $11 < L_C < 13$ μm. The enhanced values of LF-RIN and lowered values of CNR when $\eta = 0.4$ correspond to the lengths of TCC that result in unstable regular and/or irregular oscillations.

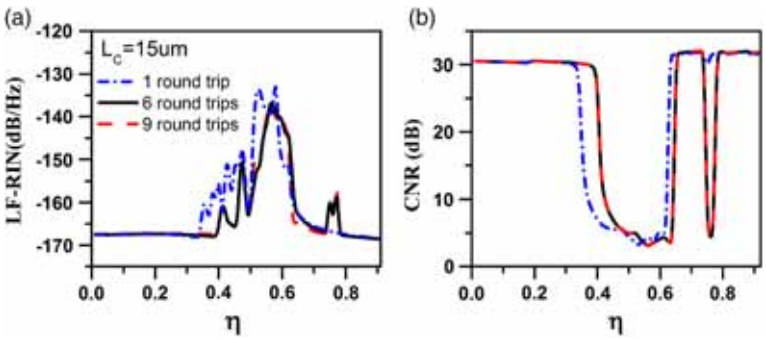

Figure 6. Plot of (**a**) LF-RIN and (**b**) CNR as functions of η in figure 5 calculated for one, six and nine round trips.

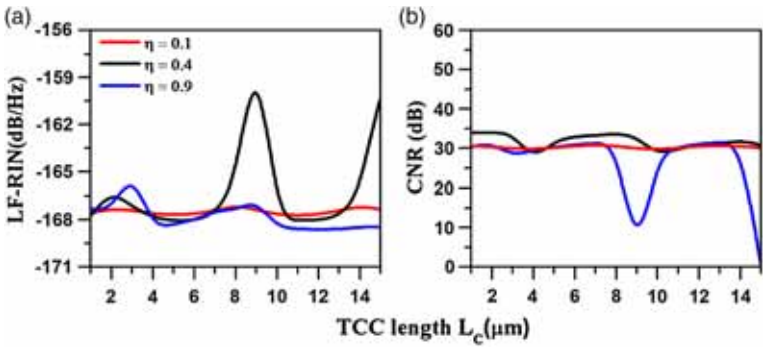

Figure 7. Variation of (**a**) LF-RIN and (**b**) CNR with L_C when $\eta = 0.1$, 0.4 and 0.9.

5. Conclusions

We modelled and illustrated the influence of slow light feedback on the noise characteristics of TCC-VCSELs. The model is valid for the strong coupling of slow light feedback and counts the material loss in the feedback cavity. We used the bifurcation diagram, temporal trajectories of the signal and the associated RIN as well as CNR to investigate and characterise the dynamic states of the TCC-VCSEL. We showed that the noise performance of the TCC-VCSEL is optimised when the TCC-VCSEL operates in CW under strong slow light feedback, which is dominant when the length of the transverse cavity is lower than 8 μm. When the TCC-VCSEL emits regular and/or irregular oscillations, RIN is enhanced and CNR is lowered.

Acknowledgements

This project was funded by the Deanship of Scientific Research (DSR), King Abdulaziz University, Jeddah, under Grant No. RG-9-130-38. The authors, therefore, acknowledge the technical and financial support of the DSR.

References

[1] K Iga, *Jpn. J. Appl. Phys.* **47**, 1 (2008)
[2] F Koyama, *J. Light. Technol.* **24**, 4502 (2006)
[3] K Kallimiani and M J O'Mahony, *IEEE J. Quantum Electron.* **34**, 1438 (1998)
[4] M Ahmed and M Yamada, *J. Appl. Phys.* **95**, 7573 (2004)
[5] N Schunk and K Petermann, *IEEE J. Quantum Electron.* **QE-24**, 1242 (1988)
[6] E Jayaprasath and S Sivaprakasam, *Pramana – J. Phys.* **89**: 76 (2017)
[7] X Zhao, D Parekh, E K Lau, H K Sung, M C Wu, W Hofmann, M C Amann and C J Chang-Hasnain, *Opt. Express* **15**, 14810 (2007)
[8] S H Lee, D Parekh, T Shindo, W Yang, P Guo, D Takahashi, N Nishiyama, C J Chang-Hasnain and S Arai, *Opt. Express* **18**, 16370 (2010)
[9] J Harrison and A Mooradian, *IEEE J. Quantum Electron.* **25**, 1152 (1989)
[10] J M Kahn, C A Burrus and G Raybon, *IEEE Photon. Technol. Lett.* **1**, 159 (1989)
[11] G Wenke, R Gross, P Meissner and E Patzak, *J. Light. Technol.* **5**, 608 (1987)
[12] G P Agrawal and C H Henry, *IEEE J. Quantum Electron.* **24**, 134 (1988)
[13] H Dalir and F Koyama, *Proceedings of the IEEE International Semiconductor Laser Conference* (2000) p. 83
[14] H Dalir and F Koyama, *IEICE Electron. Express* **8**, 1075 (2011)

[15] H Dalir and F Koyama, *Appl. Phys. Lett.* **103**, 091109 (2013)
[16] H Dalir and F Koyama, *Appl. Phys. Express* **7**, 022102 (2014)
[17] M Ahmed, A Bakry, M S Alghamdi, H Dalir and F Koyama, *Opt. Express* **23**, 15365 (2015)
[18] R Lang and K Kobayashi, *IEEE J. Quantum Electron.* **QE-16**, 347 (1980)
[19] S Abdulrhmann, M Ahmed, T Okamoto, W Ishimori and M Yamada, *IEEE J. Quantum Electron.* **9**, 1265 (2003)
[20] M Ahmed, A Bakry, M S Alghamdi and F Koyama, *Int. J. Numer. Model.* **29**, 475 (2016)
[21] M Ahmed, M Yamada and M Saito, *IEEE J. Quantum Electron.* **37**, 1600 (2001)
[22] S Abdulrhmann, M Ahmed and M Yamada, *SPIE* **4986**, 490 (2003)
[23] L A Coldren, S W Corzine and M L Mashanovitch, *Diode laser and photonic integrated circuits*, 2nd edn (Wiley, New York, 2012) p. 260
[24] G E Box and M E Muller, *Ann. Math. Statist.* **29**, 610611 (1958)
[25] A Mahmoud, M Ahmed and S W Z Mahmoud, *Pramana – J. Phys.* **90**: 61 (2018)
[26] J Ohtsubo, *Semiconductor lasers stability, instability and chaos*, 3rd edn (Springer, New York, 2013) p. 136